



EFFECT OF SIGNIFICANT ACCELERATION AND DECELERATION ON BOUNDARY LAYER PROPERTIES OF A LAMINAR FLAT PLATE

Ndivhuwo M. Musehane¹, Madeleine L. Combrinck² & Laurent Dala³

¹Department of Mechanical and Construction Engineering, Northumbria University, Newcastle Upon Tyne, NE18ST United Kingdom

Abstract

Significant acceleration and deceleration for magnitudes of the orders of $1000g/s$ occur frequently for manoeuvring ballistic projectiles. However, there are few studies in the open literature that investigate the accelerating aerodynamics for the high Mach number flow regime where unsteady peak surface pressures and temperatures can have a significant impact on the vehicle. The present study is aimed at investigating the effect of significant acceleration and deceleration on the boundary layer for a flat plate in constant linear acceleration in the hypersonic regime. Unsteady numerical simulations are carried out in an open source customised solver *ARFrhoPimpleFoam* that operates fully in the body fixed non-inertial frame. In the acceleration event, the flat plate is accelerated from steady state conditions at Mach 4 to Mach 7 at $1000g$, $10000g$ and $100000g$. In the deceleration event, the flat plate is decelerated from steady state conditions at Mach 7 to Mach 4 at $-1000g$, $-10000g$ and $-100000g$. Acceleration through the hypersonic regime resulted in cooling of the flat plate, resulting in an increase in the skin friction coefficient when compared to the same instantaneous Mach numbers for the $100000g$ magnitude. Deceleration through the hypersonic regime resulted in heating of the flat plate, resulting in an decrease in the skin friction coefficient when compared to the same instantaneous Mach numbers for the $-100000g$ magnitude. No significant changes were observed for both acceleration and deceleration through the hypersonic regime for magnitudes $1000g$, $10000g$, $-1000g$ and $-10000g$. The present results are explained using the concept of flow history

Keywords: Acceleration, Deceleration, Hypersonic, Unsteady

1. Introduction

Vehicle acceleration and deceleration for magnitudes of the orders of $100g/s$ are now commonly encountered, here $g = 9,81ms^{-2}$ is the acceleration due to gravity. The response of the surrounding compressible fluid to the vehicle acceleration and deceleration evolves in a manner different to steady state assumptions leading the vehicle to experience unsteady peak surface pressures and temperatures introducing complexity in the design of future air frames that are highly manoeuvrable and agile.

In recent decades, the effect of constant linear vehicle acceleration and deceleration has been considered mainly in the transonic [1, 2, 3, 4, 5, 6, 7] and subsonic regimes respectively [8, 9, 10, 11, 12, 13]. The unsteady formation and progression of shock waves in acceleration and deceleration has been extensively studied to a large extent and it has been shown that flow history and inertia play a pivotal role in driving the flow physics of shock waves in the transonic regime. In both the subsonic and transonic regimes results of the drag and lift forces in constant linear vehicle acceleration and deceleration deviate from steady state profiles when they are compared at the same instantaneous velocities. The focus of investigations has been on the response of the bulk flow to the vehicles acceleration and deceleration without consideration of the near surface properties.

The boundary layer determines the macroscopic surface properties such as surface shear stress, skin friction drag and heat transfer rates. The unsteady characteristics for constant linear acceleration and deceleration within the boundary layer have been investigated for subsonic flow [12]. There are however few applications in the subsonic flow regime where acceleration and deceleration magnitudes are of the orders of $100g$'s. An example of a scenario where high peak deceleration is observed is during vehicle re-entry into the earth's atmosphere. The re-entry is characterised by unsteady vehicle velocity from hypersonic to subsonic Mach numbers.

The unsteady characteristics of the hypersonic laminar boundary layer in constant linear acceleration and deceleration has not been the subject of detailed investigations. The flat plate is used in the present study for two reasons. Firstly, it is a simple idealisation of a slender body and secondly, the boundary layer is self similar and analytical solutions are available for comparison purposes [14]. The mach number range in the present investigation is between Mach 4 and Mach 7, a range where hypersonic flight has been attained.

The investigation is based on numerical simulation of a flat plate in a steady laminar compressible fluid. The computational analysis is performed using the opensource software OpenFOAM with a customised solver that operates fully in the non-inertial frame. In the non-inertial frame, the flat plate is stationary and acceleration and deceleration are achieved by addition of source terms in the conservation equations for momentum and energy which has the advantage of using a stationary mesh for accelerating motion. Details of the computational model are provided in section 2, the numerical results of the acceleration event and deceleration event are presented in section 3 and 4.

2. Computational modelling

2.1 Case description

The effect of acceleration and deceleration of a flat plate through hypersonic Mach numbers is investigated in the present study. The acceleration magnitudes chosen for the analysis are $1000g$, $10000g$ and $100000g$. The $100g$ magnitude has been used extensively in studies of acceleration through the transonic regime while the two later acceleration magnitudes are chosen to enhance the effects of acceleration and deceleration.

In the acceleration event, the flat plate is accelerated from steady state conditions at Mach 4 to Mach 7 at $1000g$, $10000g$ and $100000g$. In the deceleration event, the flat plate is decelerated from steady state conditions at Mach 7 to Mach 4 at $-1000g$, $-10000g$ and $-100000g$.

The length of the flat plate is $L = 0.1m$ and the angle of attack is zero. The surrounding air is assumed to be a perfect gas, laminar and compressible with material free stream properties given in Table 1. The Reynolds number based on the free stream properties and length of the flat plate $Re_L = \frac{\rho_\infty U_\infty(t)L}{\mu_\infty}$ ranges between $Re_L = 0.14 \times 10^6$ at Mach 4 and $Re_L = 0.24 \times 10^6$ at Mach 7.

Property	Value
$\mu_\infty [kgm^{-1}s^{-1}]$	1.48×10^{-5}
$\rho_\infty [kgm^{-3}]$	0.0174
$p_\infty [kgm^{-1}s^{-2}]$	1090.16
$T_\infty [K]$	217.82
$R [m^2s^{-2}K]$	287.68
Pr	0.69
c_p	1005
$\gamma = \frac{c_p}{c_v}$	1.4

Table 1 – Material properties and free stream conditions for hypersonic compressible laminar air.

2.2 Acceleration and deceleration using source term technique

Acceleration and deceleration are modelled in a body fixed frame. In the body fixed frame, the flat plate is stationary and the compressible fluid is accelerated or decelerated using source terms.

The governing equations are the conservation equations for mass, momentum and energy in a non-inertial frame [15, 16, 17]. Assume the flat plate is undergoing unsteady translation with velocity $\mathbf{V}(t)$, the source terms in the conservation equation for momentum \mathbf{F}_{trans} and energy \mathbf{E}_{trans} are given by equations (1) and (2).

$$\mathbf{F}_{trans} = -\hat{\rho} \frac{\partial \mathbf{V}(t)}{\partial t} \quad (1)$$

$$\begin{aligned} \mathbf{E}_{trans} &= \hat{\mathbf{u}} \cdot \mathbf{F}_{trans} \\ &= -\hat{\rho} \hat{\mathbf{u}} \cdot \frac{\partial \mathbf{V}(t)}{\partial t} \end{aligned} \quad (2)$$

Specialised treatment is required for the velocity at the farfield boundaries away from the flat plate. If the motion of the flat plate is observed from the inertial frame, the flat plate has an unsteady velocity $\mathbf{V}(t)$ while the surrounding compressible fluid is stationary with velocity $\mathbf{u}_\infty = 0$. The velocity boundary condition in the relative frame $\hat{\mathbf{u}}$ is calculated by transformation of the inertial frame velocity \mathbf{u}

$$\hat{\mathbf{u}} = \mathbf{u} - \mathbf{V}(t) \quad (3)$$

The source terms in equation (1) and (2) together with the velocity boundary condition (3) are implemented into a solver *ARFrhoPimpleFoam* that operates fully in the relative frame.

2.3 Non-inertial solver ARFrhoPimpleFOAM

The source terms are implemented in the open source toolset OpenFOAM version 6. OpenFOAM is based on the finite volume framework and has been chosen in the present study for three reasons. Firstly, the packaged solvers and utilities are freely available. Secondly, the packaged solvers and utilities are re-usable and can be customised by adding source terms, adapting boundary conditions and implementing custom thermodynamics models etc. Thirdly, the C++ library comes with a vast array of models that can be dynamically linked to a customised application, these include thermodynamics models, turbulence models, Finite Volume discretization techniques.

The *SRFPimpleFoam* application has been modified. Firstly, the solution methodology has been adapted to take into account compressible fluid. Secondly, the source terms in equations (1) and (1) have been included to take into account unsteady translation. Lastly, the specialised boundary condition in equation (3) is implemented as a derived boundary condition that switches between inflow and outflow based on the direction of the flux.

The new solver is named *ARFrhoPimpleFOAM* (Accelerating Reference Frame - rhoPimpleFoam). The solver *ARFrhoPimpleFoam* is a pressure based solver that uses the PISO (Pressure Implicit with Splitting of Operators) algorithm for the pressure velocity coupling. The solution methodology was chosen as follows, implicit Euler is used for the time discretization and second order schemes are used for the spatial discretization. The inputs required for *ARFrhoPimpleFoam* are the pressure, temperature and initial velocity. The prescribed motion of the flat plate is obtained by providing the initial and final velocity together with the initial and final time. The duration of both the acceleration and deceleration events is $9.05 \times 10^{-4}s$, $9.05 \times 10^{-3}s$ and $9.05 \times 10^{-2}s$ for magnitudes 1000g, 10000g and 100000g respectively.

2.4 Computational domain

The extent of the computational domain is depicted in Figure 1 (a). The height of the computational domain is approximately 10δ , where δ is the boundary layer thickness. The boundary conditions are fixed value at the inlet for pressure and temperature. The pressure and temperature are interpolated from the internal nodes for the Outlet and Freestream boundaries. The Plate is assigned a no slip boundary condition and a zero heat flux to set an adiabatic wall condition. The velocity boundary condition for the Inlet, Freestream and Outlet is set to the specialised velocity boundary condition named *ARFFreestreamVelocity* (Accelerating Reference Frame - FreestreamVelocity) in equation (3).

The computational mesh is refined by clustering cells in the direction normal and downstream of the flat plate. The computational mesh maintains a y^+ value of approximately one to ensure resolution

of the viscus sub-layer within the boundary layer. Mesh dependence study results are discussed in the next section.

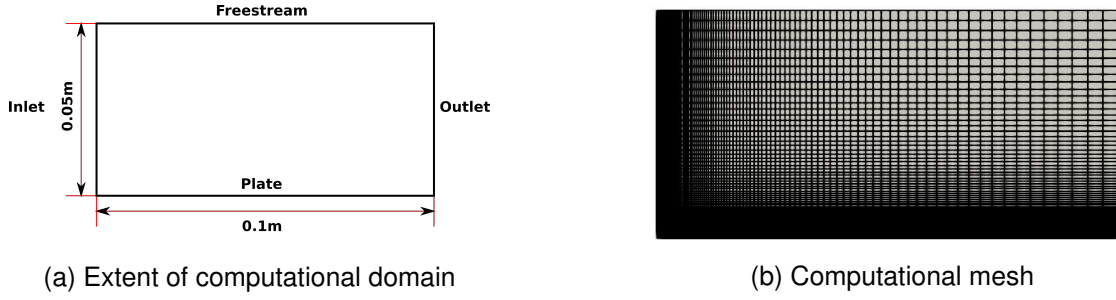


Figure 1 – Computational grid arrangement

2.5 Validation of steady state implementation

Validation of steady state operation of *ARFrhoPimpleFoam* is determined by comparing the numerical solution of velocity, temperature and skin friction profiles to the analytical closed form solutions from Monaghan [14] at Mach 7. Monaghan [14] developed closed form solutions to the self similar laminar compressible boundary layer with the assumption that the enthalpy is dependent on local flow conditions. The comparison of wall normal velocity and temperature profiles at a station $x = 0.1m$ of the flat plate is illustrated in Figure 2. Reasonable agreement is obtained for the solution of the velocity profile in the inner portion of the boundary layer. Deviation of the numerical solution is observed between $\eta = 5$ and $\eta = 20$. The difference in the adiabatic wall temperature in Figure 2b is 34.86K which represents an error of 1.77%.

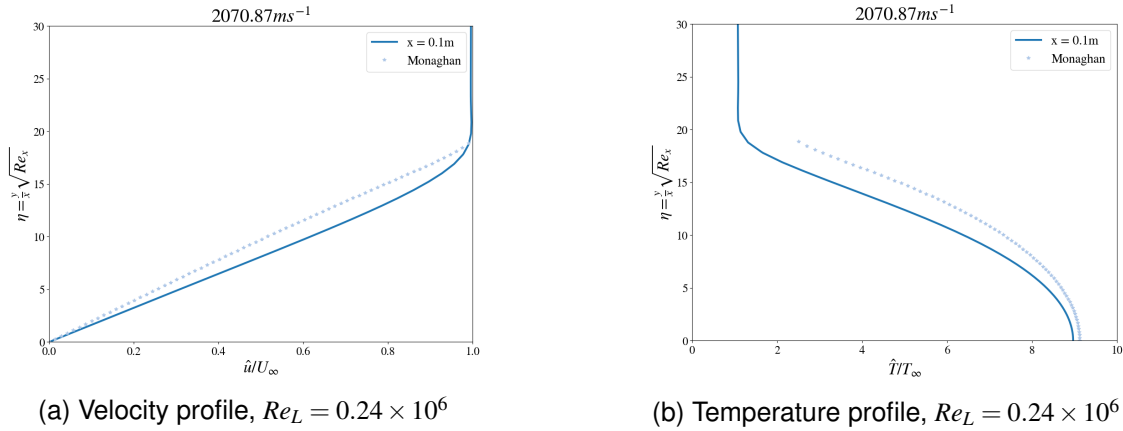


Figure 2 – *ARFrhoPimpleFoam* numerical results (solid line) compared to analytical closed form solutions (diamond).

The skin friction coefficient is calculated using equation (4), where τ_w is the wall shear stress.

$$c_f = \frac{\tau_w}{\frac{1}{2}\rho u_\infty^2} \quad (4)$$

Figure 3 compares the skin friction coefficient to results from Monaghan and the skin friction coefficient evaluated using the temperature method. In the reference temperature skin friction and Reynolds number are evaluated at a temperature $T^* = \left(1 + 0.032M_\infty^2 + 0.58\left(\frac{T_{ad}}{T_\infty} - 1\right)\right) T_\infty$ where the adiabatic wall temperature is $T_{ad} = \left(1 + \frac{\gamma-1}{2}M_\infty^2\right) T_\infty$. Reasonable agreement is obtained for the entire length of the flat plate.

3. Acceleration of flat plate

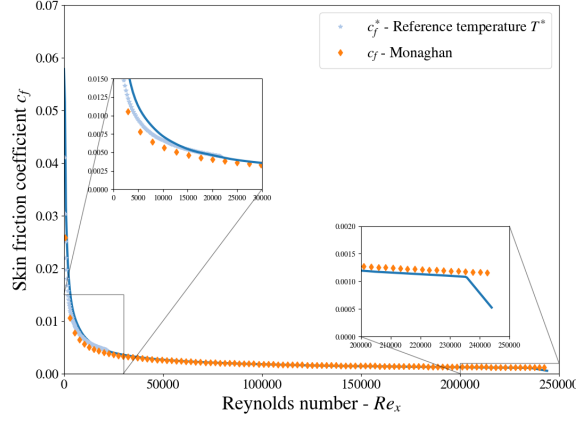


Figure 3 – Skin friction coefficient (solid line) at Mach 7 ($U_\infty = 2070.87m/s$) compared to results from Monaghan (diamond) and reference temperature method (star).

3.1 Temperature profiles

The effect of constant linear acceleration of a flat plate on the temperature profiles is presented in this section. The acceleration profile is compared to the steady state profile due to Monaghan [14] at the same instantaneous Mach numbers. The velocity at each Mach number is calculated here as $U_\infty(t) = M_\infty \sqrt{\gamma RT_\infty}$.

Figure 4 illustrates the temperature profile at instantaneous velocities during the acceleration event. The effect of acceleration is to increase the thickness of the thermal boundary layer and the adiabatic wall temperature. At the start of the acceleration event at $1193.16ms^{-1}$ there is no observable deviation in the temperature profile for all acceleration magnitudes and the steady state profile. As the acceleration event proceeds at $1222.59ms^{-1}$, the adiabatic wall temperature of the 100000g acceleration magnitude lags behind the steady state value while the remaining acceleration magnitudes have not deviated from the steady state value. The remainder of the acceleration event is characterised by a time delay in the 100000g acceleration magnitude as compared to the steady state profile.

3.1.1 Velocity profiles

The effect of constant linear acceleration to the velocity profile is presented in this section. Figure 5 illustrates the velocity in the normalised wall normal direction η during the acceleration event. A decrease in the adiabatic wall temperature in acceleration is expected to result in a thinner boundary layer.

At the start of the acceleration event at $1193.16ms^{-1}$ the velocity profile for all acceleration magnitudes and the steady state profile are the same. As the acceleration event proceeds at $1222.59ms^{-1}$, the 100000g velocity in the outer portion of the boundary layer deviates from the steady state profile. The remainder of the acceleration event is characterised by a slight deviation of the 100000g velocity as compared to the steady state profile.

3.2 Skin friction profile

The skin friction coefficient is calculated for the steady state simulations using equation (5) and for the unsteady simulations using equation (6).

$$c_f = \frac{\hat{\tau}_w}{\frac{1}{2}\rho\hat{u}_\infty^2} \quad (5)$$

$$c_f(t) = \frac{\hat{\tau}_w}{\frac{1}{2}\rho\hat{u}_\infty^2(t)} \quad (6)$$

Figure 6 illustrates the skin friction profile at two locations on the flat plate $x = 0.02m$ and $x = 0.08m$. The effect of acceleration is to decrease the skin friction coefficient as the Mach number increases during the acceleration event. However, comparison at the same instantaneous Mach number shows that the skin friction for acceleration is greater than the steady state value. Accordingly, acceleration

SIGNIFICANT ACCELERATION AND DECELERATION FOR HYPERSONIC LAMINAR BOUNDARY LAYERS

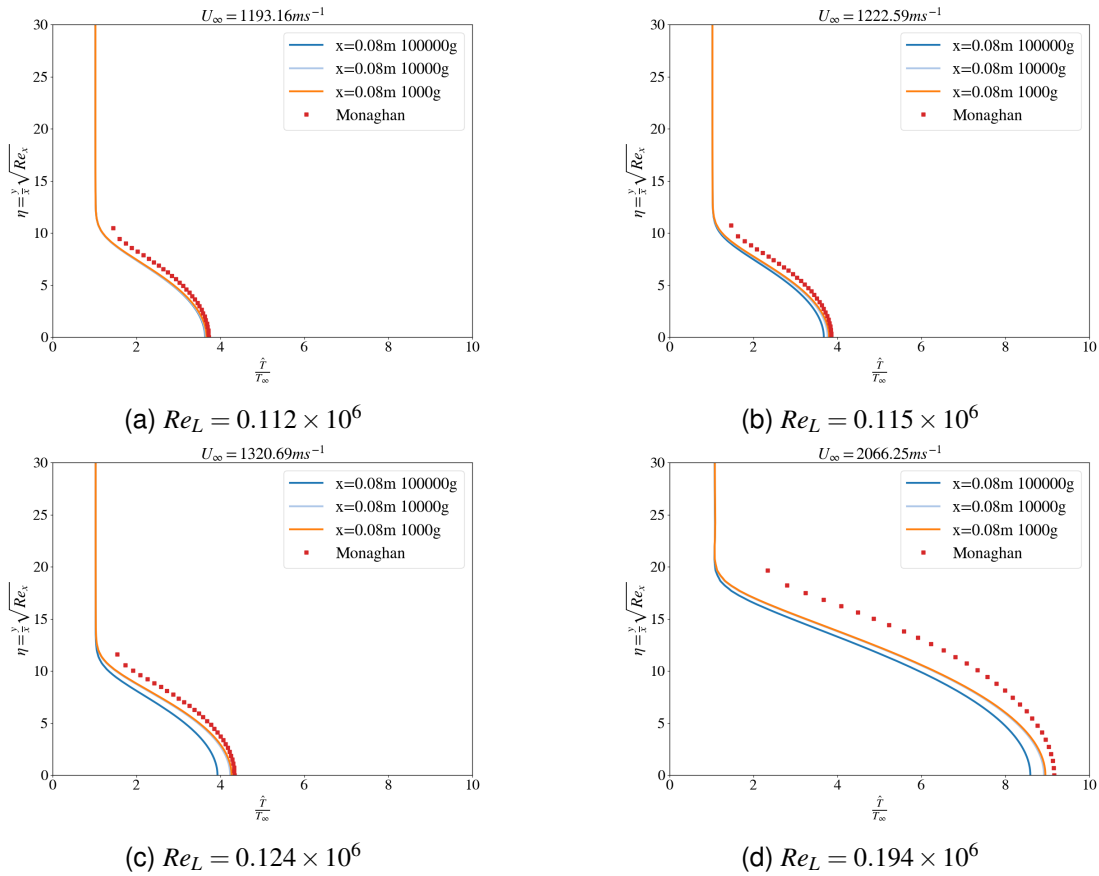


Figure 4 – Temperature profile in normalised wall normal direction η for acceleration magnitudes 100000g, 10000g and 1000g. Acceleration event proceeds from left to right.

increases the wall shear stress to a value greater than the steady state value at the same instantaneous Mach number. Changes in the skin friction coefficient are considerable at the trailing edge $x = 0.08m$ as compared to the leading edge of the flat plate $x = 0.02m$.

In the inertial perspective, as the flat plate accelerates its velocity increases rapidly and the response propagates outwards from the surface of the flat plate to the stationary farfield. The fluid closest to the flat plate is displaced outwards as the plate moves. In the non-inertial perspective, as the flat plate accelerates from Mach 4 to Mach 7 the free stream velocity increases rapidly. The external compressible fluid does not have enough time to attain steady state conditions. Due to the concept of flow history, the flow at Mach 7 contains features from lower Mach numbers at a previous time instant. This is evidenced by the acceleration wall temperature being lower than the steady state value at the end of the event at Mach 7 as illustrated in Figure 4.

4. Deceleration of flat plate

4.1 Temperature profiles

The effect of constant linear deceleration of a flat plate on the temperature profiles is presented in this section. Similar to the acceleration event, deceleration profiles are compared to the steady state profile due to Monaghan [14] at the same instantaneous Mach numbers.

Figure 7 illustrates the temperature profile at instantaneous velocities during the deceleration event. In deceleration, there is a decrease in thermal boundary layer thickness and wall temperature. The temperature profiles at four different time instants during the deceleration event show that the deceleration wall temperature is greater than the steady state value for the $-100000g$ magnitude while no significant deviation is observed for the remaining deceleration magnitudes.

SIGNIFICANT ACCELERATION AND DECELERATION FOR HYPERSONIC LAMINAR BOUNDARY LAYERS

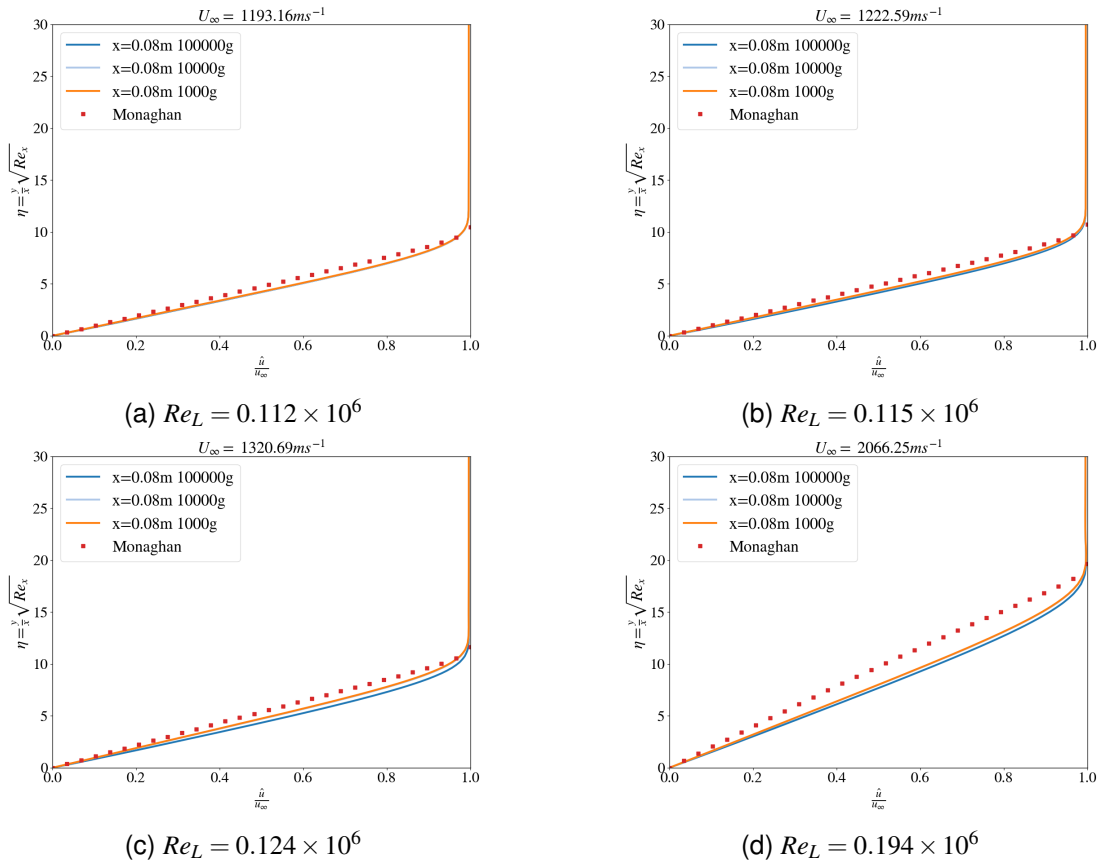


Figure 5 – Velocity profile in normalised wall normal direction η for acceleration magnitudes 100000g, 10000g and 1000g. Acceleration event proceeds from left to right.

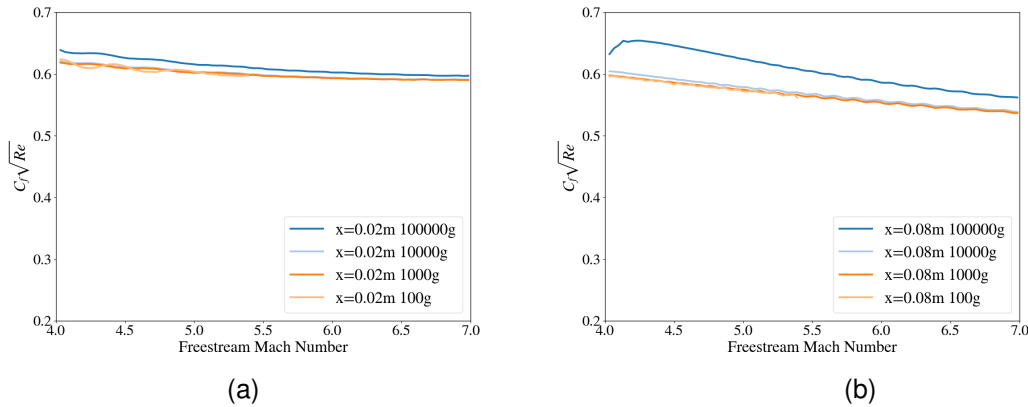


Figure 6 – Skin friction coefficient during the acceleration event at various stations down the length of the flat plate.

4.2 Velocity profiles

The effect of constant linear deceleration to the velocity profile is presented in this section. Figure 8 illustrates the velocity in the normalised wall normal direction η during the deceleration event. The effect of deceleration is to increase the thickness of the velocity boundary layer above the steady state value at instantaneous Mach numbers.

4.3 Skin friction profile

Figure 9 illustrates the skin friction profile at two locations on the flat plate $x = 0.02m$ and $x = 0.08m$ through the deceleration Mach number range. The effect of deceleration is to increase the skin friction coefficient as the Mach number decreases during the deceleration event. However, comparison at the same instantaneous Mach number shows that the deceleration skin friction is less than the

SIGNIFICANT ACCELERATION AND DECELERATION FOR HYPERSONIC LAMINAR BOUNDARY LAYERS

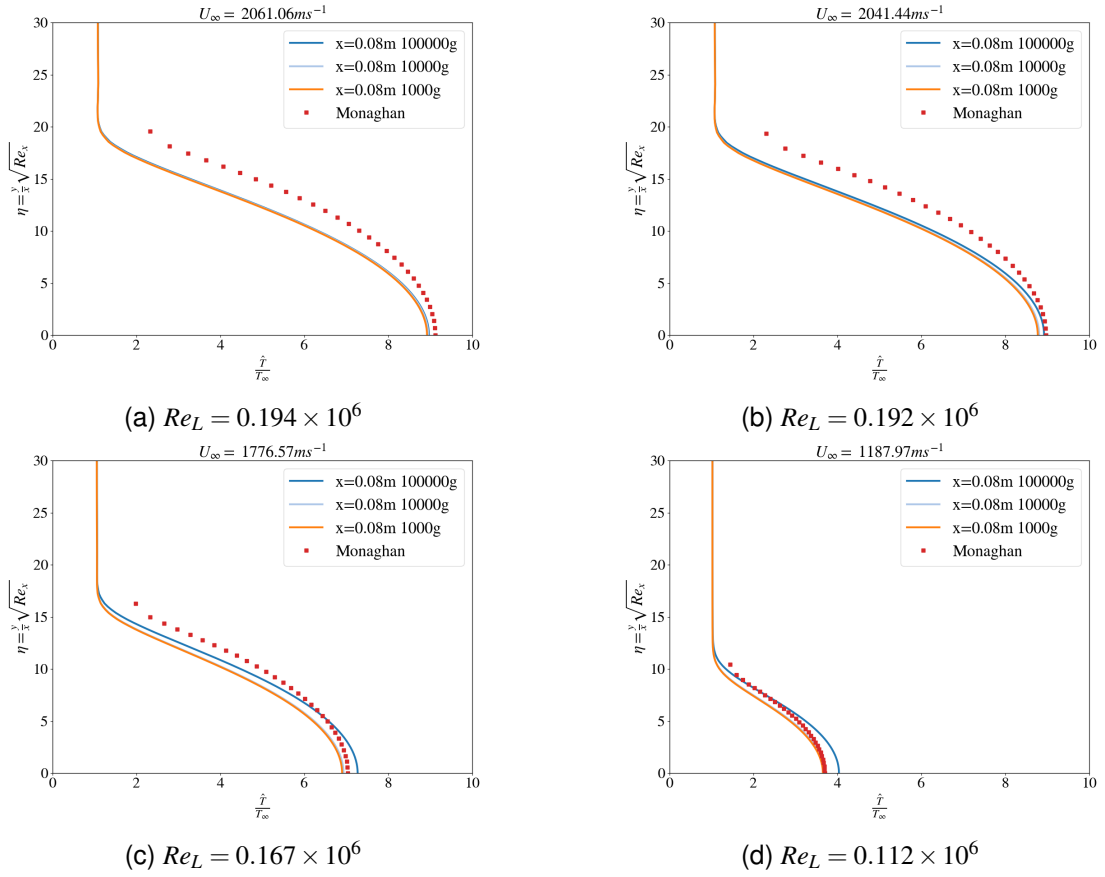


Figure 7 – Temperature profile in normalised wall normal direction η for deceleration magnitudes $-100000\mathbf{g}$, $-10000\mathbf{g}$ and $-1000\mathbf{g}$. Deceleration event proceeds from left to right.

steady state value with the significant difference observed for the $-100000\mathbf{g}$ magnitude. Accordingly, deceleration decreases the wall shear stress to a value greater than the steady state value at the same instantaneous Mach number. Changes in the skin friction coefficient are considerable at the trailing edge $x = 0.08m$ as compared to the leading edge of the flat plate $x = 0.02m$.

5. Conclusion

Numerical investigation of acceleration and deceleration of an adiabatic flat plate in a steady compressible fluid for laminar hypersonic flow has been presented. The investigation is conducted using a flow solver that operates fully in the non-inertial frame. Here, the flat plate is assumed to be stationary and the flow is accelerated and decelerated using source terms in the conservation equations for momentum and energy. The flow solver *ARFrhoPimpleFoam* has been validated for steady state operation against closed form analytical solutions for a laminar compressible adiabatic flat plate at Mach 7.

In the acceleration event, the flat plate was accelerated from steady state conditions at Mach 4 to Mach 7 at $100000\mathbf{g}$, $10000\mathbf{g}$ and $1000\mathbf{g}$. The resulting wall normal temperature, wall normal velocity and skin friction coefficient at stations on the flat plate have been determined at instantaneous Mach numbers during the event. The wall temperature in acceleration lagged behind the steady state value and maintained a magnitude lower than the steady state value when compared at the same instantaneous Mach numbers. The thickness of the acceleration thermal boundary layer is less than the steady state thickness when compared at the same Mach numbers. The acceleration velocity profiles showed thinning of the boundary layer and resulted also in a significant increase in the skin friction coefficient caused by a significant increase in the wall shear stress.

In the deceleration event, the flat plate was decelerated from steady state conditions at Mach 7 to Mach 4 at $-100000\mathbf{g}$, $-10000\mathbf{g}$ and $-1000\mathbf{g}$. The wall temperature in deceleration lagged behind the steady state value and maintained a magnitude higher than the steady state value when compared

SIGNIFICANT ACCELERATION AND DECELERATION FOR HYPERSONIC LAMINAR BOUNDARY LAYERS

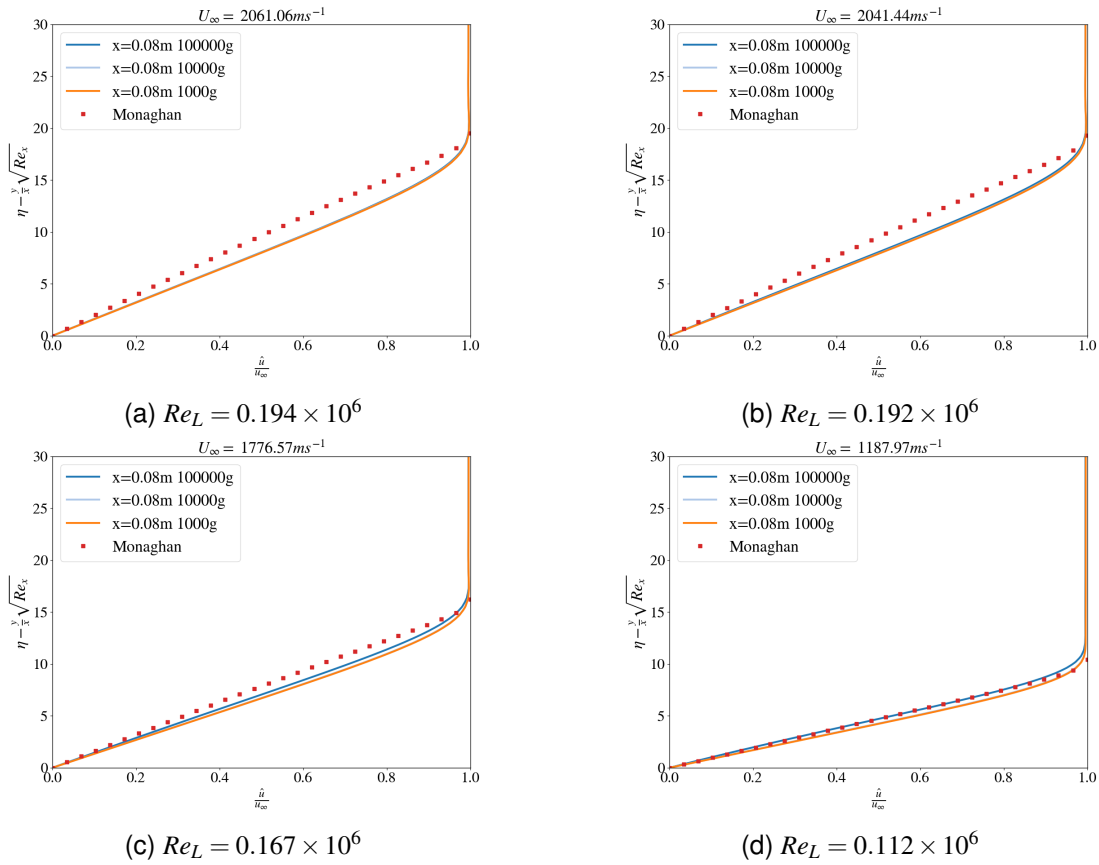


Figure 8 – Velocity profile in normalised wall normal direction η for deceleration magnitudes $-100000g$, $-10000g$ and $-1000g$. Deceleration event proceeds from left to right.

at the same instantaneous Mach numbers. The deceleration velocity profiles showed growth of the boundary layer. This resulted in an increase in the wall shear stress and increase in the skin friction coefficient.

The results of both acceleration and deceleration show in general that a high acceleration magnitude beyond current applications is required to have a considerable effect on the laminar compressible boundary layer properties for the conditions considered here. The response of both the velocity and temperature profiles through the boundary layer occurs at the start of the acceleration and deceleration event. The results suggest that pseudo steady assumptions may be an appropriate tool for determining boundary layer properties in the hypersonic flow regime. The effect of vehicle acceleration and deceleration with an increase in the angle requires further investigation. The effect of vehicle acceleration and deceleration when the air properties are variable as occurs during vehicle re-entry into the earth's atmosphere requires further investigation for cooled wall and heated wall conditions.

6. Copyright Statement

The authors confirm that they, and/or their company or organization, hold copyright on all of the original material included in this paper. The authors also confirm that they have obtained permission, from the copyright holder of any third party material included in this paper, to publish it as part of their paper. The authors confirm that they give permission, or have obtained permission from the copyright holder of this paper, for the publication and distribution of this paper as part of the AEC proceedings or as individual off-prints from the proceedings.

References

- [1] I M A Gledhill, J Baloyi, M Maserumule, K Forsberg, P Eliasson, and J Nordström. Accelerating systems: Some remarks on pitch damping. In *Fifth South African Conference on Computational and Applied Mechanics*, pages 261–274, 2006.
- [2] H. Roohani and B. W. Skews. Unsteady aerodynamic effects experienced by aerofoils during acceleration

SIGNIFICANT ACCELERATION AND DECELERATION FOR HYPERSONIC LAMINAR BOUNDARY LAYERS

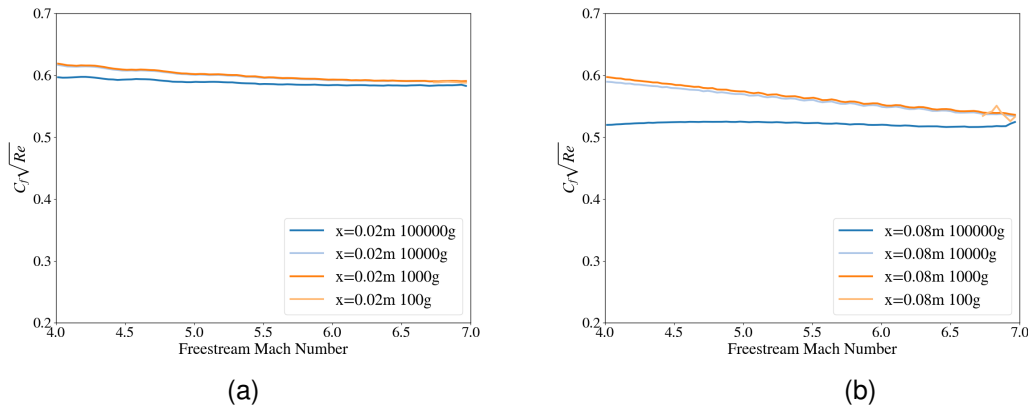


Figure 9 – Skin friction coefficient during the deceleration event at various stations down the length of the flat plate.

and retardation. *Proceedings of the Institution of Mechanical Engineers, Part G: Journal of Aerospace Engineering*, 222(5):631–636, may 2008.

- [3] Hamed Roohani and B. W. Skews. The influence of acceleration and deceleration on shock wave movement on and around aerofoils in transonic flight. *Shock Waves*, 19(4):297–305, 2009.
- [4] I.M.A. Gledhill, K. Forsberg, P. Eliasson, J. Baloyi, and J. Nordström. Investigation of acceleration effects on missile aerodynamics using computational fluid dynamics. *Aerospace Science and Technology*, 13(4):197 – 203, 2009.
- [5] I. Mahomed, Hamed Roohnai, B.W. Skews, and I.M.A. Gledhill. CFD investigation of the transonic flow-field for a decelerating axisymmetric cylinder. *R&D Journal of the South African Institution of Mechanical Engineering*, 33:85–96, 2017.
- [6] Niu Jiqiang, Sui Yang, Yu Qiujun, Cao Xiaoling, Yuan Yanping, and Yang Xiaofeng. Effect of acceleration and deceleration of a capsule train running at transonic speed on the flow and heat transfer in the tube. *Aerospace Science and Technology*, 105:105977, 2020.
- [7] I Mahomed, H Roohani, BW Skews, and IMA Gledhill. Unsteady shock wave dynamics in accelerating and decelerating flight. *The Aeronautical Journal*, pages 1–23, 2021.
- [8] Y. Lee, J. Rho, K. H. Kim, and D. H. Lee. Fundamental studies on free stream acceleration effect on drag force in bluff bodies. *J. Mech. Sci. Technol.*, 25(3):695–701, 2011.
- [9] Brett Peters and Mesbah Uddin. Impact of Longitudinal Acceleration and Deceleration on Bluff Body Wakes. *Fluids*, 4(3):158, 2019.
- [10] R Lewis, D Ludlow, and F Lendrum. Flow structure around an accelerating and decelerating vehicle. In *IMECHE International Conference on Vehicle Aerodynamics 2016: Aerodynamics by Design.*, number 1, pages 157–169, 2016.
- [11] Ting Yang and Matthew S Mason. Aerodynamic characteristics of rectangular cylinders in steady and accelerating wind flow. *Journal of Fluids and Structures*, 90:246–262, 2019.
- [12] Madeleine Lelon Combrinck. *Boundary layer response to arbitrary acceleration*. PhD thesis, University of Pretoria, 2016.
- [13] M.L. Combrinck, L.N. Dala, and I.I. Lipatov. Eulerian derivation of non-inertial navier–stokes and boundary layer equations for incompressible flow in constant pure rotation. *European Journal of Mechanics - B/Fluids*, 65:10 – 30, 2017.
- [14] R. J. Monaghan. An approximate solution of the laminar compressible boundary layer on a flat plate. Technical Report R.A.E.Tech.Note.Aero. 2025, Aeronautical Research Council, 1949.
- [15] M Combrinck, L Dala, and I Lipatov. Non-inertial forces in aero-ballistic flow and boundary layer equations. *R&D Journal*, 33:85–96, 2017.
- [16] Irvy M.A. Gledhill, Hamed Roohani, Karl Forsberg, Peter Eliasson, Beric W. Skews, and Jan Nordström. Theoretical treatment of fluid flow for accelerating bodies. *Theoretical and Computational Fluid Dynamics*, 30(5):449–467, 2016.
- [17] N.M. Musehane, M.L. Combrinck, and L.N. Dala. Eulerian derivation of the conservation equation for energy in a non-inertial frame of reference in arbitrary motion, 2021.